Supramolecular Insulating Networks Sheathing Conducting Nanowires Based on Organic Radical Cations

Hiroshi M. Yamamoto,[†,‡,*] Yosuke Kosaka,[†,‡] Ryoko Maeda,[§] Jun-ichi Yamaura,[§] Akiko Nakao,[¶] Toshikazu Nakamura,[∥] and Reizo Kato[†,‡,*]

[†]RIKEN, , [‡]JST-CREST, Wako, Saitama 351-0198, Japan, [§]Institute for Solid State Physics, University of Tokyo, Kashiwa, Chiba 277-8581, Japan, [¶]High-Energy Accelerator Research Organization (KEK), Tsukuba, Ibaraki 305-0801, Japan, and [∥]Institute for Molecular Science, Okazaki, Aichi 444-8585, Japan

ABSTRACT Six materials, $(EDT\text{-}TTF)_4BrI_2(TIE)_5$ (1, where EDT-TTF = ethylenedithiotetrathiafulvalene and TIE = tetraiodoethylene), $(EDST)_4I_3(TIE)_5$ (2, where EDST = ethylenedithiodiselenadithiafulvalene), $(MDT\text{-}TTF)_4BrI_2(TIE)_5$ (3, where MDT-TTF = methylenedithiotetrathiafulvalene), $(HMTSF)_2Cl_2(TIE)_3$ (4, where HMTSF = hexamethylenetetraselenafulvalene), $(PT)_2Cl(DFBIB)_2$ (5, where PT = bis(propylenedithio)tetrathiafulvalene and DFBIB = 1,4-difluoro-2,5-bis(iodoethynyl)benzene), and (TSF)Cl(HFTIEB) (6, where TSF = tetraselenafulvalene and HFTIEB = 1,1′,3,3′,5,5′-hexafluoro-2,2′,4,4′-tris(iodoethynyl)-biphenyl), consisting of conducting nanowires were obtained by galvanostatic oxidation of the donor molecules in the presence of the corresponding halide anions and iodine-containing neutral molecules. We report their characterizations using single-crystal crystallography, electrical resistance measurements, and electron spin resonance. The structures are built on stacks of planar cations of the donors that are isolated electrically by an insulating network consisting of supramolecular assemblies of the halide anions and neutral molecules held together by a halogen bond. The size and shape as well as the orientation (tilt) of the donors are matched by the self-organization of the insulating sheaths in all cases, providing a pea-in-a-pod example in the field of supramolecular chemistry. The observed resistivities, resistivity anisotropies, and electron spin resonance behaviors of these salts are analyzed by tight-binding band calculations and resistance-array modeling. Crystal 6 with insulating layer of 1 nm thickness exhibits 8 orders of magnitude anisotropy in its resistivity, indicating high potential of the supramolecular network as sheathing material. The observation of such networks leads us to propose a roadmap for future development toward multidimensional memory devices.

KEYWORDS: supramolecular network · halogen bond · molecular conductor · nanowire sheathing · anisotropic resistivity

Bottom-up nanotechnology is one of the key concepts for the fabrication of novel materials from the molecular scale through the nanoscale to the microscale and is expected to enable fabrication of high-density information devices at much lower cost than those made by lithographic techniques.[1] Since the molecular structures of organic molecules are synthetically controllable, their organization in the solids using supramolecular methodology should enable the design of structures on the nanometer scale.[2] Indeed, several molecular devices have been realized and proven to work as memory or logic circuits.[3] Along with the ideas of redundancy and defect-tolerant computing,[4] self-assembly of several kinds of molecules is attracting scientific interest for its potential to form a two-dimensional (2D) large-scale array of circuits. Nanowires, such as carbon nanotubes (CNTs) and inorganic semiconductor nanowires, have been good candidates in wiring these molecular devices, but the proper alignment of these building units still requires investigation. Methods based on high-voltage electric fields, in situ CNT formations, and solvent flows have been known to be able to align nanowires, but the positional accuracies of these technologies are still lacking.[5] Moreover, the wires produced are naked and tend to have short-circuits. Crystal edge printing, on the other hand, appears very promising. Although the pattern is limited in cross-bar arrangement, the accuracy of the wiring is very precise.[6] The rapid progress of recent research in the bottom-up strategy reaffirms the prospect of eventual success once certain difficulties are overcome. However, the wiring techniques in these systems will remain in 2D space for the foreseeable future as no research is currently investigating 3D wiring methods to the best of our knowledge. The advantage of 3D wiring is obvious because the number of possible devices increases not just by a power of 2 but 3. The topic of 3D wiring is, therefore, very important not only in nanotechnology but also in lithographic logic circuits, although the third dimension (*i.e.*, the number of lithographic layers) is quite limited in lithographic technology. 3D strategies for device integration in optical memory systems have also been actively discussed, but the problem of cross-talk prevents the practical implementation of such methods.[7] Although electrical devices have advantages in preventing

*Address correspondence to yhiroshi@riken.jp and reizo@riken.jp.

Received for review May 15, 2007 and accepted December 6, 2007.

Published online January 1, 2008.
10.1021/nn700035t CCC: $40.75

TABLE 1. Selected Crystallographic Data

crystal	**1**	**2**	**3**	**4**	**5**	**6**
empirical formula	$C_{42}H_{24}S_{24}Br_1I_{22}$	$C_{42}H_{24}S_{16}Se_8I_{23}$	$C_{38}H_{16}S_{24}Br_1I_{22}$	$C_{15}H_{12}Cl_1Se_4I_6$	$C_{44}H_{28}F_4Cl_1S_{16}I_4$	$C_{26}H_4F_6Cl_1Se_4I_4$
formula weight	4169.89	4592.10	4113.79	1304.98	1688.73	1289.22
crystal system	tetragonal	tetragonal	tetragonal	orthorhombic	triclinic	monoclinic
a/Å	23.435(10)	23.825(8)	23.389(4)	14.322(1)	10.596(6)	20.159(4)
b/Å				22.811(2)	17.69(1)	4.073(1)
c/Å	8.130(3)	8.088(3)	7.995(1)	7.9230(7)	7.784(4)	20.481(4)
α/deg					98.066(6)	
β/deg					94.176(10)	108.75(1)
γ/deg					100.044(8)	
V/Å^3	4465(3)	4591(3)	4374(1)	2588.4(4)	1415(1)	1592.4(7)
space group	*Pmbm* [a]	*Pmbm*	*Pmbm*	*Pbam*	$P\bar{1}$	*P*2/c
Z	2	2	2	4	1	2
D_{calcd} (D_{obs})/g cm^{-3}	3.101 (3.11(1))	3.321	3.124	3.348	1.981	2.689
$2\theta_{max}$/deg	60	60	55	70	55	55
color/shape	black/needle	black/needle	black/needle	black/needle	black/block	black/elongated block
goodness of fit	1.65	1.17	1.70	1.47	2.33	1.05
R; R_W	0.088; 0.295 [b]	0.097; 0.213 [b]	0.092; 0.252 [b]	0.064; 0.158	0.050; 0.183	0.044; 0.131

[a]This crystal was solved in $P42_12$ space group in our previous paper.[8a] It is more appropriate, however, to assign this crystal to higher-symmetry space group *Pmbm*. [b]Moderately high *R* factors for these crystals are due to the orientational disorder of donor molecules described in the main text.

cross-talk due to the greater ability of electrons to localize as compared to photons, the absence of intrinsically 3D wiring technology has kept researchers away from considering such high-density device systems.

Molecular conductors based on radical cations of tetrathiafulvalene (TTF) and its derivatives have been of major interest in the last 2 decades. Their structures are built on stacks of these flat molecules with large transfer integrals between nearest neighbors to result in band formation, where partial filling due to removal of some of the electrons provide a wide range of ground states ranging from superconducting, metallic, spin density wave, charge density wave, charge ordering, and semiconducting. With so many known examples, certain rules have been established regarding structure–property relationships. In order to expand this repertoire and to control the physical properties of molecular conductors, we have developed donor-type molecular conductors consisting of two-dimensional (2D) layers of BEDT-TTF (bis(ethylenedithio)tetrathiafulvalene) isolated by insulating supramolecular assemblies made up of iodine-containing neutral molecules and the halide counterions.[8] The neutral molecules connect counteranions through halogen bonding such as to form an infinitely assembled network in the crystals, which match the space required by the donor layers and, therefore, dictate the spacing between the molecules in the conducting layers. In the course of this work, we have noticed that the supramolecular insulating network can spatially divide and confine the conducting donor molecules not only into 2D layers but also into 1D channels. A series of compounds have been isolated which consist of a single chain of donors isolated by a 3D network of halide anions connected by weak halogen bonds with iodine-containing neutral molecules. Since the diameters of the 1D conducting moieties in these materials are on the order of nanometers, we consider these wires as good candidates for wiring in nanometer space. In addition, the 3D translational symmetry of crystal renders them potential for use in electrical circuits that enable crossed-bar addressing in 3D space.[9]

In this paper, we present six examples found to have supramolecular insulation of nanowires and an analysis of the observed conducting and insulating properties. In order to clarify the property as a nanowire, we have estimated and improved the insulation property of the supramolecular network sheathing it. In one crystal high resistivity up to 10^{13} Ω cm has been achieved in the insulating direction by increasing the thickness of the supramolecular sheath to 1 nm. This high insulation confirms the ability of the halogen

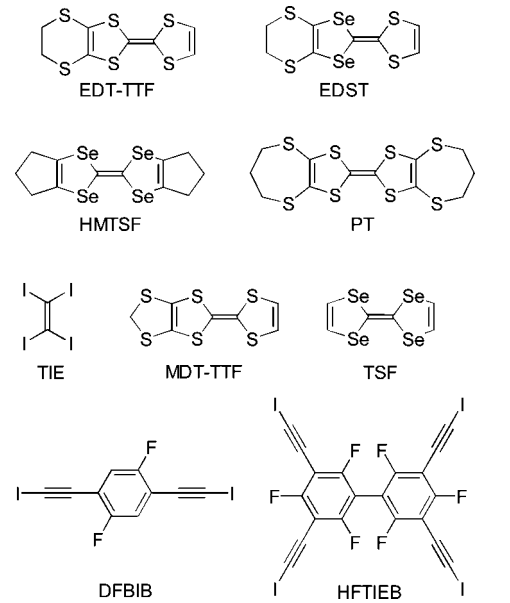

Scheme 1. Molecular Structures

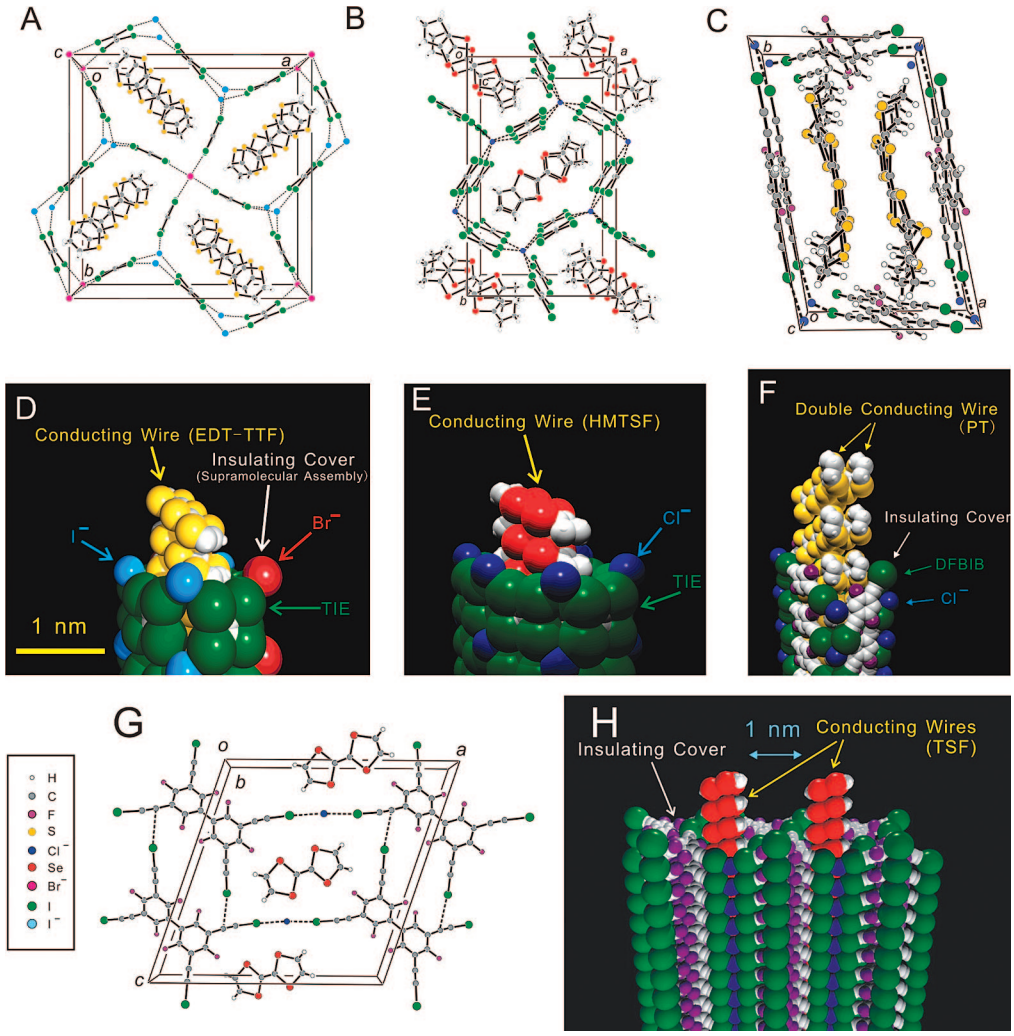

Figure 1. Crystal structures for 1 (A), 4 (B), 5 (C), and 6 (G). The dotted lines denote the "halogen bond" based on Lewis acidity of the neutral iodine atoms. The nanowire structures constructed in 1 (D), 4 (E), 5 (F), and 6 (H) are also presented in CPK modeling. White, gray, purple, yellow, blue, red, magenta, green, and sky blue denote hydrogen, carbon, fluorine, sulfur, chloride ion, selenium, bromide ion, iodine, and iodide ion in panels A–H.

bonded supramolecular network to insulate between the conducting moieties and forms the shape of the nanowire. Furthermore, a roadmap toward possible applications of these materials is proposed that includes the implementation of nanoscale wiring in 3D space that could potentially realize very high-density and large-scale memory or logic circuits in the near future.

RESULTS

Crystal Structure. The key feature of the six crystal structures for our compounds is the formation of the insulating network composed of supramolecular organization of the anions and an iodine-containing neutral molecule sheathing electrically conducting nanowires, Figure 1. The molecules used in the crystals are shown in Scheme 1.

The crystal structure of $(EDT\text{-}TTF)_4BrI_2(TIE)_5$ (**1**, where EDT-TTF = ethylenedithiotetrathiafulvalene and TIE = tetraiodoethylene), our first example for a supramolecular sheathing of 1D stack, is shown in panels A and D of Figure 1. A brief description of its structure has previously been given and here we compare it with other compounds.[8a] Crystals of $(EDST)_4I_3(TIE)_5$ (**2**, where EDST = ethylenedithiodiselenadithiafulvalene) and $(MDT\text{-}TTF)_4BrI_2(TIE)_5$ (**3**, where MDT-TTF = methylenedithiotetrathiafulvalene) exhibit the same compositions as **1** (four donors, three halides, and five structure-directing neutral molecules). Their crystal structures are also similar where donor stacks are separated by an identical 3D network. The 3D network, based on halogen bonding between halide anions and TIEs, is indicated by dotted lines in Figure 1. The halogen bond distances between the iodine atoms of TIE and halide anions are summarized in Table 2. The 1D columns of the donor molecules run through channels in the 3D network. The unit cell contains four channels, each consisting of two donor molecules in the stack direction. Two crystallographically independent TIEs could be observed in the crystal structure: one molecule, lying on a 2-fold axis and two mirror

TABLE 2. Characteristic Sizes of Supramolecular Units Based on TIE

crystal	position of TIE unit	X^-	width/Å	length/Å	$I\cdots X^-$ distance/Å	reduction [a] ratio/%
1	2-fold axis + mirror	I^-	9.5	8.1	3.74	6
	general	Br^-/I^-	9.0	8.1	3.71/3.71/3.44/3.50	3/3/13/12
2	2-fold axis + mirror	I^-	9.7	8.1	3.80	4
	general	I^-	9.2	8.1	3.71/3.74/3.55/3.55	6/6/10/10
3	2-fold axis + mirror	I^-	9.1	8.0	3.54	11
	general	Br^-/I^-	9.1	8.0	3.65/3.67/3.50/3.51	5/4/12/11
4	inversion center + mirror	Cl^-	8.3	7.9	3.20	14
	mirror	Cl^-	8.3	7.9	3.15/3.33	16/11

[a] Reduction ratios were calculated *vs* van der Waals contact.

planes, forms halogen bonds with four surrounding I^- while the other molecule is similarly surrounded by two Br^- and two I^-. In turn, one Br^- forms halogen bonds with eight surrounding TIEs while one I^- is surrounded by six TIEs. As for the donor molecules, there is an orientational disorder with two possible modes of tilting with respect to the *c* axis. The angles between the *c* axis and the normal of the donor planes are ±32° for **1**, ±29° for **2**, and ±29° for **3**. From a crystallographic point of view, the coexistence of these two orientations in one channel is unlikely. One column is expected to be composed of the donors with only one orientation. This disorder results in the observation of diffuse streaks in the *a** and *b** directions. Donor molecules in the unit cell are related to each other by a 4-fold axis and/or mirror planes.

The crystal structure of $(HMTSF)_2Cl_2(TIE)_3$ (**4**, where HMTSF = hexamethylenetetraselenafulvalene) is shown in panels B and E of Figure 1. One-half of HMTSF, one-half and one-quarter of TIE, and one-half of chloride ion (Cl^-) are crystallographically independent. The former TIE lies on a mirror plane, and the latter is located both on a mirror plane and a 2-fold axis. The $I\cdots Cl^-$ distances are given in Table 2. One TIE forms halogen bonds with four surrounding Cl^- and each Cl^- is in turn similarly surrounded by six TIEs, all through the halogen bonds indicated as dotted lines in the figure. These interactions result in the formation of the supramolecular assembly. In a similar way as for crystal **1**, the donor molecules were analyzed as the superposition of two orientationally disordered molecules. They stack with tilt angle of ±22° with respect to the *c* axis, and the stacks are separated by the insulating supramolecular assembly.

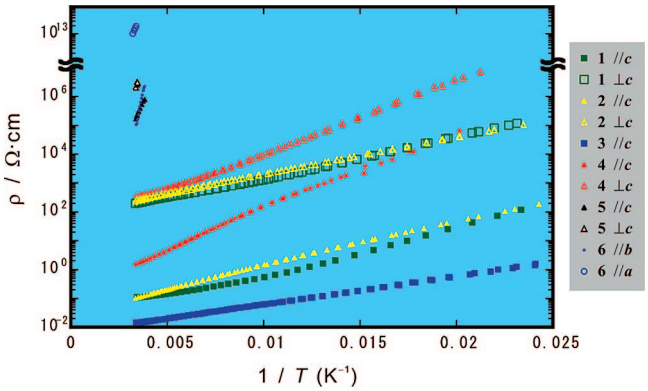

Figure 2. Temperature dependence of the resistivity for 1 (‖*c* and ⊥*c*), 2 (‖*c* and ⊥*c*), 3 (‖*c*), 4 (‖*c* and ⊥*c*), 5 (‖*c* and ⊥*c*), and 6 (‖*b* and ‖*a*).

The crystal structure of $(PT)_2Cl(DFBIB)_2$ (**5**, where PT = bis(propylenedithio)tetrathiafulvalene and DFBIB = 1,4-difluoro-2,5-bis(iodoethynyl)benzene) is shown in panels C and F of Figure 1. One whole PT, two halves of DFBIB, and one-half of Cl^- are crystallographically independent. In the unit cell, two PTs are located on general positions and are related by an inversion center. The two DFBIBs and Cl^- are on inversion centers. The $I\cdots Cl^-$ distances of 3.08 and 3.13 Å are 17% and 16%, respectively, shorter than sum of the van der Waals radii. The "double-decked" side-by-side array of donor molecules, insulated by the DFBIB-Cl^- supramolecular assembly, runs along the *c* axis without any short $S\cdots S$ contacts.

The crystal structure of (TSF)Cl(HFTIEB) (**6**, where TSF = tetraselenafulvalene and HFTIEB = 1,1′,3,3′,5,5′-hexafluoro-2,2′,4,4′-tris(iodoethynyl)-biphenyl) is shown in panels G and H of Figure 1 . Halves from each of the molecules TSF, Cl^-, and HFTIEB are crystallographically independent. The TSF donor is on an inversion center, whereas both Cl^- and HFTIEB are on 2-fold rotation axes. There are short contacts between the iodine of HFTIEB and Cl^- as well as between iodine and ethynyl carbons as shown by dotted lines in the figure. The former interaction is especially strong with a very short contact distance of 3.04 Å, 18% shorter than the sum of the van der Waals radii. In this crystal, the conducting donor molecules are also stacked in a 1D manner and insulated by the supramolecular assembly. Since the unit cell contains only one molecular stack, the donor column is uniform. It is noteworthy that the donor columns are separated from each other by 10 Å (=1 nm) along the *a*-axis direction.

Resistance measurements were performed on crystals of all the compounds. They all exhibit thermally activated behavior of their resistivity as seen in the Arrhenius plots of Figure 2. The anisotropy of the resistivity was measured for all the crystals except that of crystal of **3** whose width was not sufficient for the anisotropy measurement. Resistivity value (0.1 Ω cm at room tem-

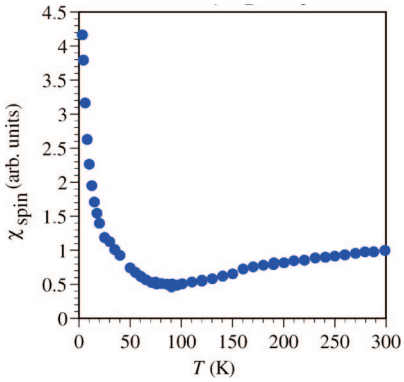

Figure 3. Temperature dependence of spin susceptibility of 1 measured by electron spin resonance.

perature) and activation energy (27 meV) for **1** and **2** are nearly identical for both the directions parallel and perpendicular to the *c* axis. The same temperature-independent $\rho(\perp c)/\rho(\parallel c)$ anisotropy value of 2000 was measured for these salts. On the other hand, lower resistivity (0.02 Ω cm at room temperature) and activation energy (19 meV) in $\rho(\parallel c)$ are observed for crystal **3**, although these three crystals have similar packing as described above. Crystal **4** also exhibited the same activation energies in the directions parallel and perpendicular to the *c* axis. For this crystal, however, the resistivity value at room temperature (1 Ω cm) is higher than those for crystals **1** and **2** along the *c*-axis direction by an order of magnitude, and its anisotropy is around 100. The activation energy is about 45 meV for both $\rho(\perp c)$ and $\rho(\parallel c)$. The resistivity of crystal **5** is even higher than that of crystal **4,** with an anisotropy of about 10. The activation energies for crystal **5** cannot be calculated exactly due to the narrow temperature range of the measurement, but the values are around 300 meV. The resistivities of crystal **6** at room temperature were 1×10^5 Ω cm in the *b*-axis direction, 5×10^5 Ω cm in the *c*-axis direction, and 1×10^{13} Ω cm in the *a*-axis direction, which means the resistivity anisotropy is 10^8 for this material (measured by three-probe method as described in Supporting Information). The activation energies for crystal **6** cannot be calculated exactly due to the narrow temperature range in which measurements could be made, but the values are around 300–500 meV in every direction.

Electron spin resonance was measured on crystal **1**. A single Lorentzian-shape signal was observed from room temperature to 4 K. The integrated signal intensity, as shown in Figure 3, shows small temperature dependence from room temperature to 30 K, below which the intensity exhibits a steep increase.

DISCUSSION

Crystal Structure. The most striking element of these compounds concerns the supramolecular chemistry of the two networks with complementary charges, the stacks of donor radical cations and the assembly of the anion and the neutral molecule, which are held together by electrostatic forces to create cocrystals. Their modes of organization depend on two independent weak chemical bondings. While the cationic donor stacks are dominated by π−π of the C−S systems, the halide anion and the iodine in the neutral molecule generate a network based on a halogen bond. The interactions between halide anions and neutral iodine atoms are a type of Lewis acid–base interaction between electron-deficient iodine (soft acid) and electron-rich halide anions (base).[10] In this report, we designate this type of coordination as the "halogen bond" even in situations where the base is not a halogen atom. The halogen bond between the halide anions and the iodine-containing neutral molecules is very strong and directional such that it always forms in the direction opposite to the carbon−iodine single bond with short contact distances. The directionality of the halogen bond gives it an advantage over other noncovalent interactions such as the hydrogen bond in that the lack of rotational degrees of freedom in the C═C−I···X− dihedral angle when compared to the more free range of motion exhibited by the C−O−H···O dihedral angle allows the construction of stronger and firmer supramolecular assemblies. The contact distances of the halogen bonds, summarized in Table 2, are 3–18% shorter than the sum of van der Waals radii of the atoms, indicating great strength in this interaction.

The magnificent outcome of the above supramolecular chemistry in these six compounds is the way in which the insulating sheath made up of the supramolecular network of the halide anions with the neutral molecules via halogen bonds organize themselves in such a way to snuggly fit the donor stack. It is also to be noted that the donor cations tilt to accommodate themselves within the network. In doing so, there is a mutual relative motion of both moieties to minimize the free energies and crystallize in the structures found. It is to be noted that we have not encountered other crystalline phases that is a common theme in radical−cation chemistry. Such cocrystal of 1D conducting stack and insulating sheath structure can be accurately described by the Corey−Pauling−Koltun model in Figure 1D.[11] This structure is surprisingly general for this series of compounds where the donor molecules such as EDST in **2**, MDT-TTF in **3**, HMTSF in **4**, PT in **5**, and TSF in **6** have different shape and size as well as different degrees of formation of hydrogen bonds.

One major difference for the general organization of the donors within the structures is that within crystals **1**, **2**, **3**, **4**, and **6** all the donors exhibit 1D columns due to their relatively planar shape but for compound **5** the donors form face-to-face pairs which are twisted by approximately 90°. These modes of packing are encountered in the structures of radical salts, as for example the κ-phases of $(BEDT\text{-}TTF)_2X$.[12] In most cases, 1D stacking is the more frequent packing motif for

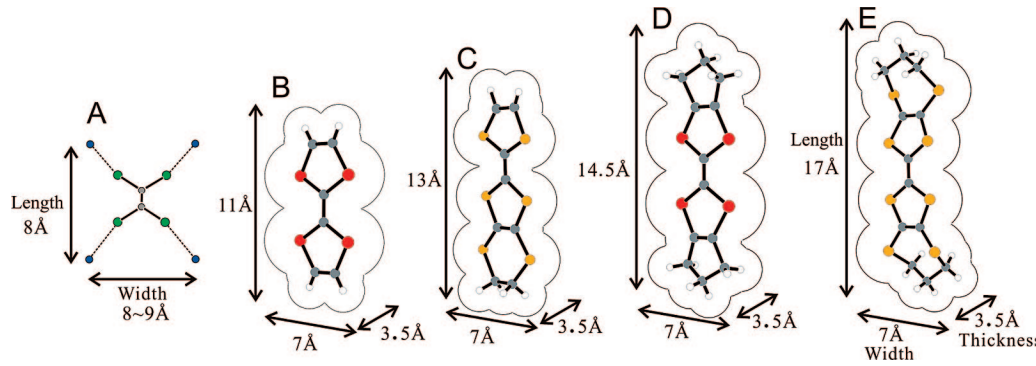

Figure 4. Dimension definitions for the TIE unit (A), TSF (B), EDT-TTF (C), HMTSF (D), and PT (E). The van der Waals outlines are drawn for the donor molecules.

these planar molecules due to the directional $\pi-\pi$ interactions. For the PT molecules of crystal **5**, however, $\pi-\pi$ interactions should not be the only explanation for the nanowire structure. Another driving force in the formation of these crystals is that the supramolecular network structure is strong and flexible to allow for the formation of channel structures similar to other architectures such as those in metal-based coordination polymers.[13] Along with this characteristic, the flexibilities in both the coordination number and angles around the anions are also important factors for the generation of the observed supramolecular structures (see also Table 2 in ref 8a and Supplementary Figure S3). Indeed, the coordination number around the halide ions ranges from two (in crystal **6**) to eight (in crystals **1**, **2**, and **3**). This flexibility is undoubtedly necessary for forming square channels in crystals **5** and **6**, pentagonal channels in crystals **1**, **2**, and **3**, and hexagonal channels in crystal **4**. The above three factors are, however, insufficient to explain the formation of crystalline entities in *multicomponent* supramolecular materials. As we discussed previously, the most important factor for the formation of multicomponent supramolecular crystals is the compatibility between the conducting donor molecule and the supramolecular building units.[8a] In the following discussion, analyses of the present anionic network structures will allow a better understanding as to how compatibility can be realized in these materials.

This compatibility can be examined by first analyzing crystal **1**. As mentioned in Results, EDT-TTF in the 1D channels exhibits tilt with respect to the *c* axis despite not having this tendency in the known radical salts. A search of Cambridge Crystallographic Database for EDT-TTF cation radical salts resulted in less than 30 hits, where 1D column structure with the tilt angle of less than 5° is most dominant.[14] In the present case, EDT-TTF of crystal **1** shows a tilt of $\pm 32°$ for it to be accommodated within the supramolecular network. Because of the nature of the halogen bond, the size of the TIE unit as defined in Figure 4A restricts the donor period along the *c* axis to approximately 8 Å so that the donors maintain compatibility with TIE units. However, the thickness (interplanar distance) of the EDT-TTF is about 3.5 Å, which is not an integer fraction of 8 Å. For this reason, EDT-TTFs in the column slip along their longitudinal axis to accommodate the repeating period of the supramolecular assembly. At the same time, the longitudinal size of the donor column fits the longer diameter of the pentagonal channel (Figure 5A). This display of compatibility is very subtle and selective. An important example of compatibility can also be observed when comparing the fine details of the structures **1** and **3**. Because MDT-TTF is slightly smaller than EDT-TTF, it only has to tilt by 29° to maintain compatibility. In tandem, the TIE unit shrinks both in length (8.1 $\rightarrow$ 8.0 Å) and width (9.5 $\rightarrow$ 9.1 Å: see Table 2). "Fine tuning" of compatibilities can again be observed when crystals of **1** and **2** are compared; EDST is slightly larger than EDT-TTF, and thus the size of TIE unit is increased by substituting Br^- with I^- such that the width of the TIE unit becomes 9.7 Å and EDST more snuggly fits the wider channel. It is noteworthy that $(EDT\text{-}TTF)_4I_3(TIE)_5$, $(EDST)_4BrI_2(TIE)_5$, and $(MDT\text{-}TTF)_4I_3(TIE)_5$ form well-developed optically reflecting crystals but their mosaicity is quite large for high-quality structure determinations.

Another example of compatibility can be seen in the hexagonal channel structure constructed in crystal **4**. The supramolecular network structure consists of hexagonal instead of pentagonal 1D channels to accommodate the HMTSF. Because HMTSF is much longer than EDT-TTF, EDST, or MDT-TTF, it is no longer compatible with the pentagonal channel even with increasing the tilt angle of the donor column as with crystal **1**. Consequently, the channel adopts hexagonal instead of pentagonal (Figure 5B) and the tilt of HMTSF is 22° to facilitate the compatibility between the two components. This flexibility exhibited by the supramolecular assembly originates from the variability of the coordination number around the anion. It is notable that the donor:anion ratio changes from 4:3 to 1:1 with this geometric change, thus altering the band filling of the donor electronic structure.

For crystal **5**, the square channel is composed of four DFBIBs and four Cl^-. The size of the channel is,

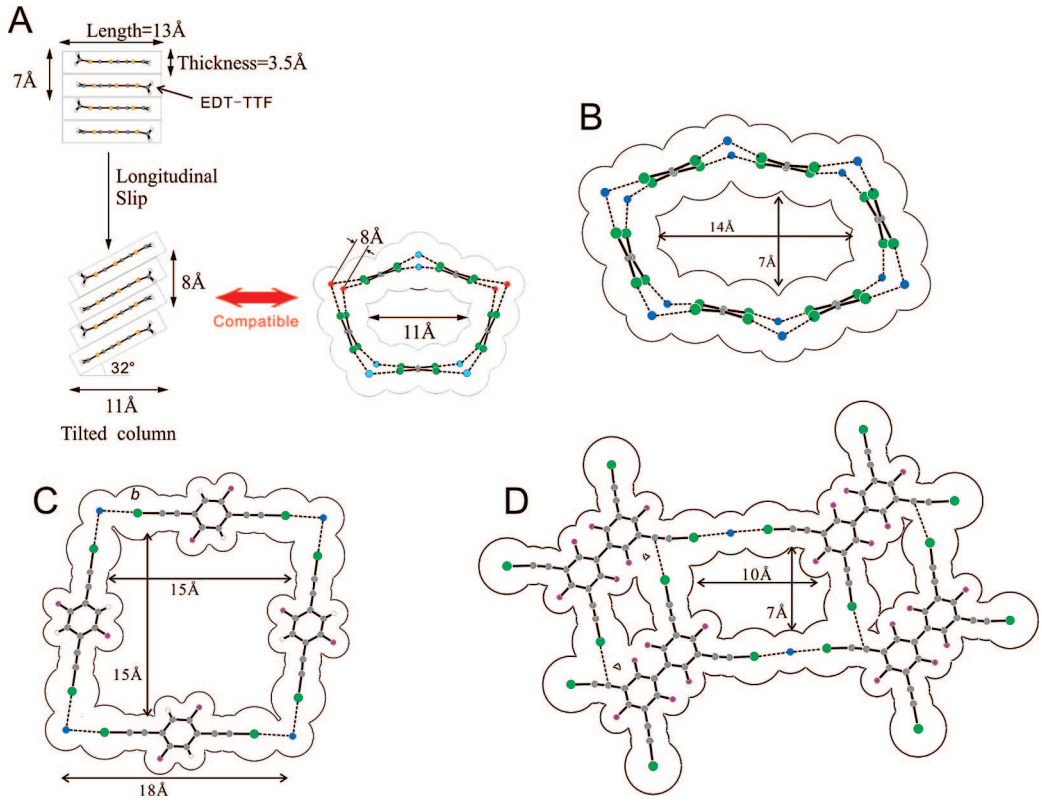

Figure 5. The structures of supramolecular assemblies with van der Waals outlines. The assemblies show pentagonal- (A), hexagonal- (B), and parallelogram-shaped (C and D) channels in crystals 1, 4, 5, and 6, respectively. In part A, the structure of the donor column in 1 is also presented in order to explain how compatibility is accomplished between the supramolecular assembly and the tilted donor column.

however, too large to accommodate PT donors if the channel opens parallel to the *c* axis: The size of the channel is 15 × 15 Å (Figure 5C) which is far larger than the double-decked PT donors (7 Å in thickness). Consequently, the supramolecular square plane is not parallel to the (0, 0, 1) plane but to the (2, 1, $\bar{1}$) plane as shown in Supplementary Figure S1. This high incline of the supramolecular assembly allows crystal compatibility between donors and the anionic network. Meanwhile, the PT dimers are moderately tilted sideways with respect to the *c* axis so that their long bodies (17 Å) fit the channel width (15 Å).

In crystal **6**, the supramolecular assembly is formed by the I···C interaction (3.54 Å) as well as the I···Cl^- interaction. Because the iodine atom of HFTIEB is a Lewis acid, the interacting bases are not necessarily halide anions but π electrons of sp carbon. Indeed, we have reported several acid–base interactions between electron-deficient iodine and sulfur, (neutral) fluorine, gold, or sp^2 carbon in previous works.[8,55] This I···C interaction allows the supramolecular assembly to form a rectangular channel of 7 × 10 Å size (Figure 5D) to accomplish compatibility between TSF and the anionic network, instead of forming the 10 × 10 Å square channel shown in Supplementary Figure S2. Speculatively, although it is possible for HFTIEB molecules to form square channels only by halogen bonding with Cl^- as shown in Supplementary Figure S2, the size of such channels is probably incompatible with that of TSF donors.

Band Calculation and Conduction Properties. Band structures, which are based on the tight-binding approximation using transfer integrals from extended Hückel molecular orbital calculation, were calculated for all the salts. The calculated overlap integrals are listed in Table 3 as well as in the caption for Figure 6. It is notable that the overlap integrals between the stacks are less than 10^{-6} due to the spatial separation by the supramolecular sheath. It is known that the typical 1D conductor TTF-TCNQ, whose resistivity anisotropy is about 100, shows interstack overlap integral of the order of 10^{-4}.[15] The lack of interstack interaction should be the reason for anisotropic resistivity exhibited by the present materials, especially in crystal **6**. The anisotropy values should be, however, potentially higher than the observed ones because the present resistivity in the wire direction contains the resistance of the supramolecular network, according to the discussion in

TABLE 3. Overlap Integrals ($S/10^{-3}$) between HOMOs of Donor Molecules in 1, 2, 3, 4, and 6[a]

	1	2	3	4	6
S(*c*1) (inner-cell)	−31.5	−15.4	−10.1	−9.3	N.A.
S(*c*2) (intercell)	−18.7	−15.9	−11.4	−4.3	−7.0

[a]The interstack overlap integrals are well below the calculation accuracy ($<10^{-6}$).

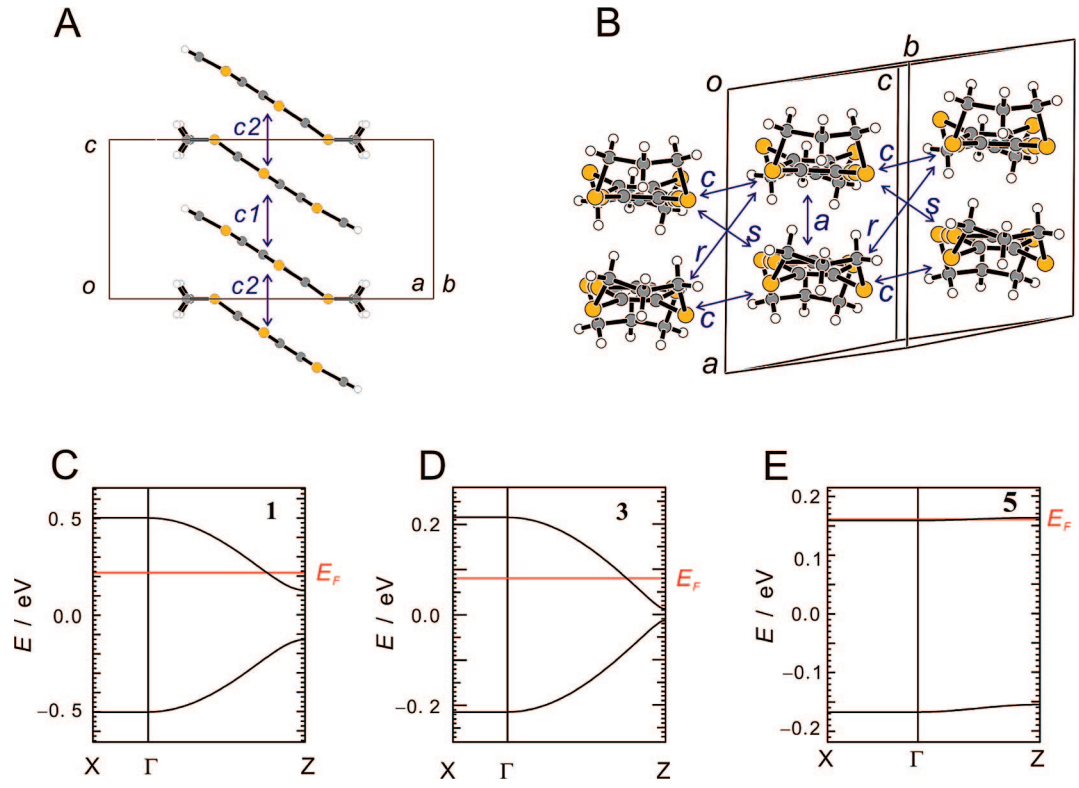

Figure 6. (A) The donor arrangement in crystal 1, along with the indexes for overlap interactions. (B) The donor arrangement in crystal 5, along with the indexes for overlap interactions. The calculated overlap integrals ($S/10^{-3}$) are as follows: $S(a) = -15.89$, $S(c) = -0.55$, $S(r) = 0.004$, $S(s) = -0.09$. (C, D, and E) Calculated band dispersions for 1, 3, and 5, respectively.

the following section. The crystals for **1**, **2**, **3**, **4**, and **5** show dimerized 1D band structures. Because the valence of the donors for **1**, **2**, and **3** are +3/4, the fillings for these HOMO bands are 5/8. The band structures are those of conductors with featureless 1D Fermi surfaces. Consequently, the wires should be metallic, as indicated in Figure 6C, Supplementary Figure S6A, and Figure 6D.

The results of the resistance measurements can be interpreted on the basis of the above band calculation. The resistivity parallel to the *c* axis ($\|c$) for crystal **1** is 0.1 Ω cm, while that perpendicular to the *c* axis ($\perp c$) is 200 Ω cm at room temperature. The high anisotropy of 2000 apparently originates from the molecular wire-bundle structure that prevents current flow perpendicular to the *c* axis. Despite very anisotropic conduction, the activation energies are almost identical for both directions. This coincidence of the same activation energies for both $\|c$ and $\perp c$ directions is not insignificant because the band calculation determines that the material has metallic band filling along the *c* axis for crystals **1**, **2**, and **3** (*i.e.*, the resistivity should *decrease* with the temperature) while there is no effective transfer integral perpendicular to the *c* axis (*i.e.*, the resistivity should *increase* when the temperature is decreased). This phenomenon is also known to be true of the platinum complex $K_2Pt(CN)_4Br_{0.3} \cdot nH_2O$ (so-called KCP) and is due to lattice defects that limit the conduction along the *c* axis, effectively cutting the wire.[16,17]

Assuming that resistance values are determined solely by the hopping between the wires because the resistance of the wires is negligible when compared to that of the insulating sheath (TIE), the conduction anisotropy analysis can be performed based on the resistance-array model. Such an assumption is theoretically supported by the above tight-binding band calculation that predicts metallic conduction for wires. A kind of mean-field approximation along with several additional assumptions of which details are described in Supporting Information estimates the resistivity along the *c* axis ($\rho(\|c)$) at $2Ra^2/5cx^2$, where *a* and *c* are cell parameters, *R* is resistance of TIE, and *x* is the average number of cells between two lattice defects in the wire. The *R* values are assumed to be identical for the sake of simplicity in the calculation, although two crystallographically distinct TIE molecules occur in the crystal. Similarly, the resisitivity perpendicular to the *c* axis ($\rho(\perp c)$) can be calculated as $3Rc/8$. These formulas determine why the same activation energies are observed for both $\rho(\|c)$ and $\rho(\perp c)$, as both resistivity values are proportional to *R* (and *a*, *c*, and *x* are almost temperature independent). Because the resistance *R* originates from the phonon-assisted hopping process between neighboring wires, its value can be written as $\alpha[\exp(E_a/kT)]$, where α is a constant and E_a is the activation energy for hopping. Because the same hopping process and therefore the same resistivity-determining step exists for both $\|c$ and $\perp c$ directions, the same activation

energy also exists in both directions. As such, the anisotropy $\rho(\perp c)/\rho(\parallel c)$ can be calculated as a temperature-independent constant $15c^2x^2/16a^2$. From the experimental data, the anisotropy is about 2000, and therefore x can be estimated as approximately 130. Thus, a defect fatal to wire conduction is present every 260 donor molecules within one column since two donor molecules are stacked in a wire in the unit cell. This defect density is in good agreement with known defect density values of 0.1–1% measured for other kinds of molecular conductors and provides fundamental data for further development of crystalline supramolecular nanowires.[18] Whether these defects are responsible for the slight deviation from Arrhenius plots for **1**, **2**, **3**, and **4** is currently not well defined. The deviation can also be attributed both to the effect of thermal contraction and to the metallic character of the wire moiety.

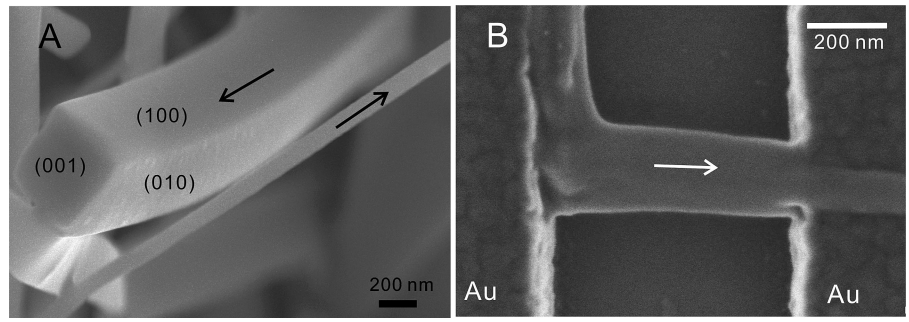

Figure 7. (A) SEM (scanning electron microscope) image for needle-shaped nanocrystals of 1. The square (001) section reflects the tetragonal symmetry of the crystal. The arrows indicate the *c* axis directions of the crystals. The thinnest crystal (100 nm thickness) contains about 10000 wires. (B) Nanocrystal of 1 bridging two gold electrodes (center).

The above analysis, which indicates that the molecular wires are fragmented in the crystal, is consistent with other measurements. The electron spin resonance (ESR) measurements can be explained by attributing the weak temperature dependence above 30 K to the Pauli paramagnetic behavior of the metallic nanowires and the steep increase in spin susceptibility below 30 K to the weak localization of the conduction carriers. A possible explanation for this weak localization is that the independent molecular wires are too short to allow for continuous band dispersions resulting in bands composed of discontinuous levels separated by small energies. Because the bandwidth for this material as determined from band calculations is 0.4 eV and the number of unit cells in each fragment is 130, the energy separation can be estimated as ~3 meV (=0.4 eV/130 cells). This energy separation can be converted to a temperature of 30 K, which is on the same order of carrier localization observed in ESR measurements. Additional support for our interpretation is described in another recent report from our group where resistance measurements along the *c* axis for a very short (100 nm) single crystal of **1** demonstrate the conductivity is retained down to 4 K.[19] This kind of measurement has been done on crystals directly grown on electrodes deposited on SiO_2/Si substrates as shown in Figure 7. The bias voltage for these measurements (about 10 mV/unit cell) was large enough to overcome the discontinuity (*ca*. Three meV) between levels in the band. Thus, a crystal of **1** may not necessarily be an insulator if it is so short that a fatal lattice defect does not have the probability to occur.

The cause for the lower resistivity and activation energy for crystal **3** is not yet apparent, but the analysis above suggests that it may be found in the hopping process between wires. The HOMO of MDT-TTF is known to have moderate contribution from the terminal methylene carbon while the HOMO of EDT-TTF has no contributions from terminal methylene carbons. Therefore, hopping between wires seems to be enhanced as compared to crystals **1** and **2**.[20]

The band filling for crystal **4** is 1/2 because the valence of the donor is +1, thus making the wire band insulator (Supplementary Figure S6B). Note that the valence difference of HMTSF compared to the crystals **1**, **2**, and **3** is due to the geometric change of the channel from pentagonal to hexagonal. Although the wire in crystal **4** is an insulator due to its specific band filling, the coincidence of the same activation energies for both $\rho(\parallel c)$ and $\rho(\perp c)$ seems to be due to the same reason as for crystal **1**.

The band filling for the upper branch of the band for crystal **5** is 1/2, but the small overlap along the *c* axis causes the band widths to be very narrow (<0.01 eV) and not wide enough for band conduction, causing this salt to probably be in a Mott-insulating state.

The band for crystal **6** is a simple cosine function because the donor stack is uniform. Considering that the band filling is 1/2, and the on-site Coulomb for the donor is very large compared to the bandwidth (0.2 eV), the wire should also be an insulator. The high resistivity values of these crystals even along the wire support this speculation. For crystal **6**, the thickness of the insulating sheath has been successfully increased to ~1 nm by using HFTIEB, resulting in the high insulation resistance of 10^{13} Ω cm along the *a* axis (perpendicular to the donor stacking axis). This value is comparable to epoxy resin, which suggests that the supramolecular assemblies made of iodine-containing neutral molecules provide good electrical insulation for the molecular conducting wires. To the best of our knowledge, a conduction anisotropy of 10^8 ($=10^{13}/10^5$) is the highest value recorded for single chemical substance at room temperature. From a magnetic point of view, crystal **6**

is expected to be a very pure 1D Heisenberg spin system.

Roadmap for Development of the Supramolecular Nanowires. For the present compounds all the supramolecular insulating networks have their channels disposed in one direction. The one-dimensional nature of the present compounds is due partly to the nature of the neutral molecule and the properties of the halogen bond. Thus, all the conducting wires are aligned in one direction. In order to fabricate more practical and high-density systems, one should look for compounds having their channels in two or three dimensions for cross-bar wiring material in the *3D crystal space* as shown in the example in Supplementary Figure S8.[9] It should be possible to generate such 2D or 3D channels by developing the chemistry of iodine-containing neutral molecules with the appropriate geometries and number of iodine. With the knowledge acquired for the iodine-containing neutral molecules used in the present work, we should be able to design 2D and 3D systems. As far as we know, this type of high-density 3D wiring utilizing 3D translational symmetry of crystal has not been proposed yet. Therefore, we discuss briefly this possibility in the following section as well as in the Supporting Information.

Five main issues need to be addressed for the nanowires to be practically functional: (1) multiplication of the conduction path (*i.e.*, donor column) in one wire; (2) production of thicker, more insulating covers; (3) orthogonal arrangement of the wires; (4) integration of the molecular devices; and (5) organization of an anti-cross-talk system. These conditions are based on the conduction mechanism of the nanowires discussed in the previous section. Here we focus on the former two issues in the main text because they are essential to interpret points which the crystal structures of **5** and **6** raise, and we describe the details for the latter three issues in the Supporting Information.

First of all, the wires should be almost free of defects that induce hopping between the wires. Due to the defect-tolerant concept, not all the wires need to be perfectly conducting in redundant information systems, but the yield of wires that connect one end of the crystal to the other end without the occurrence of a disconnection needs to be at least 90%, practically speaking.[4] To achieve conduction from one face of the crystal to the opposite face, it is often effective to increase the number of conduction paths in one wire. Provided that the crystal length is 1 mm, and the stacking period of the donor molecule is 4 Å, approximately 2500000 molecules are stacked in one wire. When the defect density is 1/260, one wire contains about 10000 defects on average. However, if the number of donor columns and, thus, the conduction paths are multiplied for one wire, the probability of a disconnection occurring for the entire wiring system is expected to decrease exponentially with the number of paths. For example, if the wire is doubled as in crystal **5**, the probability of a disconnection occurring becomes $1/(260)^2$ which is still too high to make such wires feasible for practical usage. But further increasing the number of conduction pathways to as many as six produces yields of 99.999999% ($=1 - 2500000/(260)^6$) that allow the connection of two ends of a crystal by crystalline nanowires without the occurrence of fatal conduction blockades. Of course, the occurrences of different defects may not be completely independent, and thus, the above estimated yield should in reality be lower. However, it should still be no less than 90%, our estimated requirement for efficient conduction.

Of secondary consideration is to increase the resistance of the insulating sheath so that electrons do not hop from wire to wire. For a first-order approximation, the hopping probability is proportional to the overlap integral between the HOMOs for the donor molecules in adjacent wires. Because the overlap integral diminishes exponentially as a function of distance, thickening of the wire cover should be significantly more effective for insulation. Such a method already achieved partial success in crystal **6** where the nearly 10 Å (1 nm) distance between wires along the *a* axis proved to be highly insulating. It is somewhat interesting that the insulation did not seem to be fatally broken by lattice defects even though they should occur in the insulation layer for crystal **6** as well. Speculatively, most lattice defects are probably insulating due to the localization effect. Nevertheless, according to the above discussions, crystals **5** and **6** are the prototypes for multiwire structures and highly insulated wires, respectively. For further discussions on 3D wiring systems, see the last section of the Supporting Information.

CONCLUSION

In this work, we have demonstrated the ability of the insulating supramolecular network of halide anions and iodine-containing neutral molecules to organize and match the shape, size, and mode of packing of organic π radicals and prevent carrier hopping between the π-radical stacks. This extension of our previous work based on layered compounds resulted in solely one-dimensional conducting nanowires. The present results highlight the importance of insulating networks that divide the conducting $\pi-\pi$ stacks into independent nanowires. The halogen bond which is rarely used in supramolecular chemistry and points to the high directionality of this bond helps in designing novel structures. In the present study we have focused not only on the conduction properties but also on the insulation property of the materials. It should be noted that the conducting donor molecules involved in these materials are very common ones, but the insulating supramolecular network defines the external form of the conducting moiety as inde-

pendent nanowire shape. This is in contrast to the material development of molecular conductors so far where the strongest emphasis is put on the development of novel conducting donor molecules. There is an interesting analogy to the contemporary electronics where the development of novel high *k* dielectrics that enable smaller gate leak current is more eagerly pursued than the material for conducting device itself.[21] In organic field effect transistors, there is also strong demand for the high OFF resistance to improve the device property. As these examples point out, it should become more and more important to control the internal/external shape, size, resistance, and dielectric permittivity of the insulating moiety. While certain existing rules on the mode of organization of the donors are well respected, in one case an unexpected double strand is observed. The transverse resistance in the crystals is increased by 10 orders of magnitude with increase of thickness of the insulating sheath from 3 Å (for **1**−**3**) to 10 Å (for **6**). The observed conducting properties were theoretically modeled and lead us to propose a procedure to fabricate more sophisticated devices with high-capacity memory.

METHODS

Materials. EDT-TTF,[22] EDST,[23] MDT-TTF,[24] HMTSF,[25] PT,[26] TSF,[27] and DFBIB[28] were synthesized as described in previous literature. The synthetic procedures for HFTIEB are described in Supporting Information. Chlorobenzene, methanol, tetraphenylphosphonium chloride, tetraphenylphosphonium bromide, and tetrabutylammonium iodide were purchased from Wako Chem. Co. Ltd., and TIE was purchased from Aldrich Chem. Co. These materials were used without further purification.

Crystal Preparation. Galvanostatic oxidation of the donor molecules dissolved in 20 mL of solutions containing neutral molecules and supporting electrolytes were performed under an argon atmosphere for a few days to as many as 25 days. Standard H-shaped cells (20 mL) and platinum electrodes (1 mm in diameter) were used for these electrolyses. Detailed conditions are summarized in Supplementary Table S1. Crystals of good quality for resistivity measurements and X-ray structure analyses were harvested from the anode. Although crystals of $(EDT\text{-}TTF)_4I_3(TIE)_5$, $(EDST)_4BrI_2(TIE)_5$, and $(MDT\text{-}TTF)_4I_3(TIE)_5$ could be prepared, their crystal quality was poor.

X-ray Analysis. Each of the selected single crystals of the six compounds was mounted on glass fibers using epoxy cement. X-ray diffraction data were collected on a MAC Science automatic four-circle diffractometer (MXC18), a Rigaku automatic four-circle diffractometer (AFC6S), or a Rigaku CCD system (Mercury) with graphite-monochromated Mo Kα radiation at 293 K. The intensities were corrected for Lorentz and polarization effects. The structures were solved by direct methods and refined by SHELXL-93 (for crystals **1**, **3**, **4**, and **6**), SHELXL-97 (for crystal **2**), or by the full-matrix least-squares method (for crystal **5**).[29] Anisotropic thermal parameters were used for non-hydrogen atoms. All hydrogen atoms were added in calculated positions with fixed isotropic contributions. All calculations were performed with use of the teXsan crystallographic software package from Molecular Structure Co. Table 1 gives selected crystal data for the six compounds. CCDC 653150−653155 contain the supplementary crystallographic data for this paper. These data can be obtained free of charge from The Cambridge Crystallographic Data Centre via www.ccdc.cam.ac.uk/data_request/cif.

Resistivity Measurement. The dc resistivity measurements were performed by the standard four-probe method except for crystal **6** in the *a* axis direction for which measurement was performed with the three-probe method as described in Supporting Information. Gold leads (10 μm or 15 μm diameter) were attached to the crystal with carbon paste.

ESR Measurement. The electron spin resonance measurements were carried out for aligned single crystals of **1** using an X-band spectrometer, Bruker ESP-300E, equipped with a rectangular cavity, TE_{011}. The temperature range of the measurements was between 300 and 4 K. The magnetic field was applied perpendicular to the *c* axis direction. A least-squares method was applied for the analyses of the observed ESR absorption derivative curves. The values of the resonance field, peak-to-peak height I_{pp} and peak-to-peak line width ΔH_{pp} were used as the fitting parameters.

Band Calculation. In order to determine intermolecular overlap integrals, HOMO obtained by the extended Hückel MO calculation was used.[15,30] The calculation was carried out with the use of semiempirical parameters for Slater-type atomic orbitals (Supplementary Table S2). It was assumed that the transfer integral (t) is proportional to the overlap integral (S), $t = \epsilon S$ ($\epsilon = -10$ eV, ϵ is a constant of the order of the orbital energies of HOMO). The band structures were calculated based on the tight-binding approximation.

SEM Image. The nano-/microsized crystals of **1** were electrochemically grown on gold electrodes deposited on a SiO_2/Si substrate. The detail of the sample preparation is described in refs 19 and S6. The images of thin crystals on the electrodes are taken by using Hitachi FE-SEM S-4800.

Acknowledgment. This work was partially supported by a Grant-In-Aid for Scientific Research (No. 16GS0219) from the Ministry of Education, Culture, Sports, Science and Technology of Japan. The authors are grateful to Dr. K. Tsukagoshi (RIKEN) for his kind offer to use the parameter analyzer, Keithley 4200-SCS.

Supporting Information Available: Synthesis of HFTIEB, additional figures for the structures of supramolecular assemblies, calculations of the anisotropic resistivity based on resistance-array model, band calculations for crystals **2**, **4**, and **6**, measurement procedures for the three-probe method, roadmap for development of the supramolecular nanowires, conditions for crystal preparation, semiempirical parameters for Slater-type atomic orbitals, and CIF files. This information is available free of charge *via* the Internet at http://pubs.acs.org.

REFERENCES AND NOTES

1. Reed, M. A.; Zhou, C.; Muller, C. J.; Burgin, T. P.; Tour, J. M. Conductance of a molecular junction. *Science* **1997**, *278*, 252–254.
2. (a) Lehn, J.-M. *Supramolecular Chemistry: Concepts and Perspectives*; VCH: Weinheim, 1995. (b) Desiraju, G. R. Chemistry beyond the molecule. *Nature* **2001**, *412*, 397–400. (c) Sakurai, K.; Uezu, K.; Numata, M.; Hasegawa, T.; Li, C.; Kaneko, K.; Shinkai, S. β-1,3-Glucan polysaccharides as novel one-dimensional hosts for DNA/RNA, conjugated polymers and nanoparticles. *Chem. Commun.* **2005**, 4383–4398. (d) Pluth, M. D.; Bergman, R. G.; Raymond, K. N. Acid catalysis in basic solution: a supramolecular host promotes orthoformate hydrolysis. *Science* **2007**, *316*, 85–88.
3. Luo, Y.; Collier, C. P.; Jeppesen, J. O.; Nielsen, K. A.; Delonno, E.; Ho, G.; Perkins, J.; Tseng, H. -R.; Yamamoto, T.; Stoddart, J. F.; Heath, J. R. Two-dimensional molecular electronics circuits. *ChemPhysChem* **2002**, *3*, 519–525.
4. (a) Collier, C. P.; Wong, E. W.; Belohradsky, M.; Raymo, F. M.; Stoddart, J. F.; Kuekes, P. J.; Williams, R. S.; Heath, J. R. Electronically configurable molecular-based logic gates. *Science* **1999**, *285*, 391–394. (b) Heath, J. R.; Kuekes, P. J.;

Snider, G. S.; Williams, R. S. A defect-tolerant computer architecture: opportunities for nanotechnology. *Science* **1998**, *280*, 1716–1721.
5. (a) Hu, J.; Odom, T. W.; Lieber, C. M. Chemistry and physics in one dimension: synthesis and properties of nanowires and nanotubes. *Acc. Chem. Res.* **1999**, *32*, 435–445. (b) Duan, X.; Huang, Y.; Cui, Y.; Wang, J.; Lieber, C. M. Indium phosphide nanowires as building blocks for nanoscale electronic and optoelectronic devices. *Nature* **2001**, *409*, 66. (c) Wei, B. Q.; Vajtai, R.; Jung, Y.; Ward, J.; Zhang, R.; Ramanath, G.; Ajayan, P. M. Microfabrication technology: organized assembly of carbon nanotubes. *Nature* **2002**, *416*, 495. (d) Huang, Y.; Duan, X.; Wei, Q.; Lieber, C. M. Directed assembly of one-dimensional nanostructures into functional networks. *Science* **2001**, *291*, 630–633.
6. Melosh, N. A.; Boukai, A.; Diana, F.; Gerardot, B.; Badolato, A.; Petroff, P. M.; Heath, J. R. Ultrahigh-density nanowire lattices and circuits. *Science* **2003**, *300*, 112–115.
7. Parthenopoulos, D. A.; Rentzepis, P. M. Three-dimensional optical storage memory. *Science* **1989**, *245*, 843–845.
8. (a) Yamamoto, H. M.; Yamaura, J. -I.; Kato, R. Multicomponent molecular conductors with supramolecular assembly: iodine-containing neutral molecules as building blocks. *J. Am. Chem. Soc.* **1998**, *120*, 5905–5913. (b) Yamamoto, H. M.; Yamaura, J.-I.; Kato, R. Preparation of multicomponent molecular conductors with supramolecular assembly. *Synth. Met.* **1999**, *102*, 1448–1451. (c) Yamamoto, H. M.; Kato, R. Design, preparation, and characterization of novel et salts with supramolecular assembly. *Chem. Lett.* **2000**, 970–971. (d) Kosaka, Y.; Yamamoto, H. M.; Nakao, A.; Kato, R. Multicomponent molecular conductors with supramolecular assemblies prepared from neutral iodine-bearing *p*BIB (*p*-bis(iodoethynyl)benzene) and derivatives. *Bull. Chem. Soc. Jpn.* **2006**, *79*, 1148–1154.
9. O'Keeffe, M.; Andersson, S. Rod packings and crystal chemistry. *Acta Crystallogr.* **1977**, *A33*, 914–923.
10. (a) McDaniel, D. H.; Dieters, R. M. The CCl_5^- species. *J. Am. Chem. Soc.* **1966**, *88*, 2607–2608. (b) Creighton, J. A.; Thomas, K. M. Preparation and structures of halide-ion complexes of carbon tetrahalides and tetrahaloethylenes. *J. Chem. Soc., Dalton Trans.* **1972**, 403–410. (c) Awwadi, F. F.; Willet, R. D.; Peterson, K. A.; Twamley, B. The nature of halogen. . .halide synthons: theoretical and crystallographic studies. *J. Phys. Chem. A* **2007**, *111*, 2319–2328. (d) PyykkôStrong closed-shell interactions in inorganic chemistry. *Chem. Rev.* **1997**, *97*, 597–636. (e) Svensson, P. H.; Kloo, L. Synthesis, structure, and bonding in polyiodide and metal iodide-iodine systems. *Chem. Rev.* **2003**, *103*, 1649–1684. (f) Marks, T. J. Rational synthesis of unidimensional solids: chemical and physical studies of mixed-valence polyiodides. *Ann. N.Y. Acad. Sci.* **1978**, *313*, 594–616.
11. (a) Corey, R. B.; Pauling, L. Molecular models of amino acids, peptides, and proteins. *Rev. Sci. Instrum.* **1953**, *24*, 621–627. (b) Koltun, W. L. Precision space-filling atomic models. *Biopolymers* **1965**, *3*, 665–679.
12. (a) Kobayashi, A.; Kato, R.; Kobayashi, H.; Moriyama, S.; Nishio, Y.; Kajita, K.; Sasaki, W. Crystal and electronic structures of a new molecular superconductor, κ-(BEDT-TTF)$_2$I$_3$. *Chem. Lett.* **1987**, 459–462. (b) Urayama, H.; Yamochi, H.; Saito, G.; Nozawa, K.; Sugano, T.; Kinoshita, M.; Sato, S.; Oshima, K.; Kawamoto, A.; Tanaka, J. A new ambient pressure organic superconductor based on BEDT-TTF with T_c higher than 10 K (T_c = 10.4 K). *Chem. Lett.* **1988**, 55–58.
13. (a) Kitagawa, S.; Uemura, K. Dynamic porous properties of coordination polymers inspired by hydrogen bonds. *Chem. Soc. Rev.* **2005**, *34*, 109–119. (b) Bradshaw, D.; Claridge, J. B.; Cussen, E. J.; Prior, T. J.; Rosseinsky, M. J. Design, chirality, and flexibility in nanoporous molecule-based materials. *Acc. Chem. Res.* **2005**, *38*, 273–282. (c) Sudik, A. C.; Cote, A. P.; Wong-Foy, G.; O'Keeffe, M.; Yaghi, O. M. A metal-organic framework with a hierarchical system of pores and tetrahedral building blocks. *Angew. Chem., Int. Ed.* **2006**, *45*, 2528–2533.
14. (a) Kazheva, O.; Canadell, E.; Kushch, L.; Aleksandrov, G.; Chekhlov, A.; Buravov, L.; Dyachenko, O. New Molecular conductors based on edt with anionic complexes of rare-earth elements: (EDT)$_2$[Ho(NCS)$_4$(H$_2$O)$_4$] and (EDT)$_3$[Y(NO$_3$)$_5$]. *Synth. Met.* **2004**, *143*, 221. (b) Mori, H.; Sakurai, N.; Tanaka, S.; Moriyama, H. Crystal structures and magnetic properties of d-pπ organic conductors, (EDT-TTF)$_4$CoCl$_4$(1,1,2-TCE)$_x$ and related materials. *Bull. Chem. Soc. Jpn.* **1999**, *72*, 683. (c) Sato, A.; Ojima, E.; Kobayashi, H.; Kobayashi, A. Structural, electrical and magnetic properties of low-dimensional conductors based on unsymmetrical π donor EDT-TTF and analogous selenium-substituted molecules. *J. Mater. Chem.* **1999**, *9*, 2365. (d) Hountas, A.; Terzis, A.; Papavassiliou, G. C.; Hilti, B.; Burkle, M.; Meyer, C. W.; Zambounis, J. Structures of the new superconductor (MDT-TTF)$_2$AuI$_2$ (T_c = 4.5 K) and the organic metal (EDT-TTF)$_2$AuI$_2$ (MDT-TTF = methylenedithiotetrathiafulvalene and EDT-TTF = ethylenedithiotetrathiafulvalene). *Acta Crystallogr., Sect. C* **1990**, *46*, 228. (e) Terzis, A.; Hountas, A.; Papavassiliou, G. C.; Hilti, B.; Pfeiffer, J. Structures and conductivities of the synthetic metal salts of ethylenedithiotetrathiafulvalene (EDT-TTF) and ethylenedithiodiselenadithiafulvalene (EDT-DSDTF): 211-(EDT-TTF)$_2$IBr$_2$, 211-(EDT-DSDTF)$_2$IBr$_2$ and 212-(EDT-TTF)$_2$AuBr$_2$. *Acta Crystallogr., Sect. C* **1990**, *46*, 224. (f) Kobayashi, A.; Sato, A.; Kawano, K.; Naito, T.; Kobayashi, H.; Watanabe, T. Origin of the resistivity anomalies of (EDT-TTF)[M(dmit)$_2$](M = Ni, Pd). *J. Mater. Chem.* **1995**, *5*, 1671.
15. Berlinsky, A. J.; Carolan, J. F.; Weiler, L. Band structure parameters for solid TTF-TCNQ [tetrathiofulvalene-tetracyanoquinodimethane]. *Solid State Commun.* **1974**, *15*, 795–801.
16. The reason for the nonmetallic behavior of ρ(‖c) can also be explained by Peierls instability. But we have observed no superlattice along the *c*-axis in X-ray measurement that is expected to appear in the presence of the charge density wave. In addition, there is no reason for the activation energies to be identical in both ‖c and ⊥c directions unless the effect of lattice defects is considered.
17. (a) Bernasconi, J.; Kuse, D.; Rice, M. J.; Zeller, H. R. One-dimensional conduction. two-dimensional problem. *J. Phys. C* **1972**, *5*, L127–130. (b) Zeller, H. R.; Beck, A. Anisotropy of the electrical conductivity in the one-dimensional conductor K$_2$[Pt(CN)$_4$]Br$_{0.30}$ · 3(H$_2$O). *J. Phys. Chem. Solids* **1974**, *35*, 77–80.
18. Analytis, J. G.; Ardavan, A.; Blundell, S. J.; Owen, R. L.; Garman, E. F.; Jeynes, C.; Powell, B. J. Effect of irradiation-induced disorder on the conductivity and critical temperature of the organic superconductor κ-(BEDT-TTF)$_2$Cu(SCN)$_2$. *Phys. Rev. Lett.* **2006**, *96*, 177002/1–177002/4. (b) Forro, L.; Zuppiroli, L.; Pouget, J. P.; Bechgaard, K. X-ray diffuse-scattering study of the pinned charge-density waves in tetramethyltetraselenafulvalene dimethyltetracyanoquinodimethane (TMTSF-DMTCNQ) disordered by irradiation. *Phys. Rev. B* **1983**, *27*, 7600–7610.
19. Yamamoto, H. M.; Ito, H.; Shigeto, K.; Yagi, I.; Tsukagoshi, K.; Kato, R. Nano-size molecular conductors on silicon substrate -toward device integration of conductive CT salts. *J. Low Temp. Phys.* **2006**, *142*, 215–220.
20. (a) Kanoda, K.; Yobayashi, Y.; Takahashi, T.; Inukai, T.; Saito, G. Evidence of a spin-density-wave transition in the organic conductor (methylenedithiotetrathiafulvalene)$_2$Au(CN)$_2$ [(MDT-TTF)$_2$Au(CN)$_2$]. *Phys. Rev. B* **1990**, *42*, 8678–8681. (b) Kanoda, K.; Kato, K.; Kobayashi, Y.; Kato, M.; Takahashi, T.; Oshima, K.; Hilti, B.; Zambounis, J. Upper critical field and NMR relaxation studies of an organic superconductor, κ-(MDT-TTF)$_2$AuI$_2$. *Synth. Met.* **1993**, *55–57*, 2871–2876.
21. Banerjee, K; Mehrotra, A. Global (interconnect) warming. *IEEE, Circuits Devices Mag.* **2001**, *17*, 16–32.

22. Kato, R.; Kobayashi, H.; Kobayashi, A. Dimensionality examination of cation radical salts based on EDT-TTF(EDT-TTF = etylenedithiotetrathiafulvalene). *Chem. Lett.* **1989**, 781–784.
23. Sato, A.; Ojima, E.; Kobayashi, H.; Kobayashi, A. Structural, electrical and magnetic properties of low-dimensional conductors based on unsymmetrical donor EDT-TTF and analogous selenium-substituted molecules. *J. Mater. Chem.* **1999**, *9*, 2365–2371.
24. Papavassiliou, G. C.; Zambounis, J. S.; Mousdis, G. A.; Gionis, V.; Yiannopoulos, S. Y. Bis(alkylthio)tetrathiafulvalenes and a few of their salts. *Mol. Cryst. Liq. Cryst.* **1988**, *156* (Pt. A), 269–276.
25. McCullough, R. D.; Cowan, D. O. A convenient synthesis of hexamethylenetetraselenafulvalene (HMTSF). *J. Org. Chem.* **1985**, *50*, 4646–4648.
26. Mizuno, M.; Garito, A. F.; Cava, M. P. Organic metals: alkylthio substitution effects in tetrathiafulvalene-tetracyanoquinodimethane charge-transfer complexes. *J. Chem. Soc., Chem. Commun.* **1978**, *1*, 18–19.
27. Takimiya, K.; Morikami, A.; Otsubo, T. A convenient preparation of 1,3-dithiole-2-thione and 1,3-diselenole-2-selone derivatives. *Synlett* **1997**, 319–321.
28. Yamamoto, H. M.; Maeda, R.; Yamaura, J.-I; Kato, R. Structural and physical properties of conducting cation radical salts containing supramolecular assemblies based on p-bis(iodoethynyl)benzene derivatives. *J. Mater. Chem.* **2001**, *11*, 1034–1041.
29. Sheldrick, G. M., *Program for the Refinement of Crystal Structures*; University of Göettingen: Göettingen, Germany.
30. Mori, T.; Kobayashi, A.; Sasaki, Y.; Kobayashi, H.; Saito, G. The intermolecular interaction of tetrathiafulvalene and bis(ethylenedithio)tetrathiafulvalene in organic metals. calculation of orbital overlaps and models of energy-band structures. *Bull. Chem. Soc. Jpn.* **1984**, *57*, 627.